High-Pressure Synthesis and Properties of Solid Solutions between $BiMnO_3$ and $BiScO_3$

Alexei A. Belik,*,† Tadahiro Yokosawa,‡ Koji Kimoto,‡ Yoshio Matsui,‡ and Eiji Takayama-Muromachi†

Advanced Nano Materials Laboratory (ANML) and High Voltage Electron Microscopy Station (HVEMS), National Institute for Materials Science (NIMS), 1-1 Namiki, Tsukuba, Ibaraki 305-0044, Japan

Received November 20, 2006. Revised Manuscript Received January 16, 2007

Solid solutions $BiMn_{1-x}Sc_xO_3$ ($0 \le x \le 1$) were prepared at 6 GPa and 1383−1443 K. Selected area and convergent beam electron diffraction showed that $BiMn_{0.9}Sc_{0.1}O_3$ crystallizes in the centrosymmetric space group $C2/c$ at room temperature. The structure parameters of $BiMn_{0.9}Sc_{0.1}O_3$ were refined by the Rietveld method from laboratory X-ray diffraction data ($Z = 8$; $a = 9.6029(3)$ Å, $b = 5.60988(14)$ Å, $c = 9.7690(3)$ Å, $\beta = 108.775(2)°$) at 293 K). The Mn−O bond lengths suggest that the orbital order present in $BiMnO_3$ at 300 K disappears in $BiMn_{0.9}Sc_{0.1}O_3$. Therefore, the monoclinic-to-monoclinic phase transition observed in $BiMnO_3$ at 474 K and associated with the orbital melting was not detected in $BiMn_{1-x}Sc_xO_3$ for $x \ge 0.05$ down to 133 K. $BiMn_{1-x}Sc_xO_3$ were characterized by dc and ac magnetization, specific heat, and differential scanning calorimetry measurements. The long-range ferromagnetic order seems to survive for $x = 0-0.2$. For $x \ge 0.4$, the samples showed spin-glass-like features. The Weiss temperature deduced from the fitting of magnetic susceptibilities was positive for all the compositions with $x < 1$ and decreased monotonically with increasing x. The temperature of the magnetic transitions decreased and the temperature of the structural monoclinic-to-orthorhombic phase transition increased (from 768 K for $x = 0$ to 840 K for $x = 0.3$) with increasing x.

1. Introduction

Perovskite-like compounds with the formula of ABO_3 continue to attract a lot of attention because of the rich and fascinating physical properties on the one hand and the simple composition on the other that makes them ideal model systems for theoretical understanding of their properties. Bi-containing perovskites have received renewed interest in recent years as multiferroic materials[1−3] and lead-free ferroelectrics.[4−6]

$BiMnO_3$ is a unique compound among $BiBO_3$, where B is a magnetic ion, because $BiMnO_3$ is the only compound that shows true ferromagnetic ordering at $T_M = 99-105$ K.[7−9] In all other compounds, $BiCrO_3$,[7,10] $BiFeO_3$,[11] $BiCoO_3$,[3] and $BiNiO_3$,[12] antiferromagnetic ordering is realized with a weak ferromagnetic component in some cases due to spin canting. In addition, orbital degrees of freedom are active in $BiMnO_3$.[13,14] The long-range orbital order in $BiMnO_3$ was proposed from the analysis of the crystal structure studied by neutron diffraction[8,15] and recently confirmed by resonant X-ray scattering studies.[14] It was suggested that the ferromagnetism of $BiMnO_3$ stems directly from orbital order.[8] The measurement of ferroelectric polarization of $BiMnO_3$ was reported in only one paper.[16] Despite the preparation of highly resistive $BiMnO_3$ thin films,[17] there are no other direct confirmations (observations of $P-E$ hysteresis loops) of the ferroelectric properties of $BiMnO_3$.

* To whom correspondence should be addressed. E-mail: Alexei.BELIK@nims.go.jp.
† ANML, NIMS.
‡ HVEMS, NIMS.

(1) For recent reviews see (a) Ramesh, R.; Spaldin, N. A. *Nat. Mater.* **2007**, *6*, 21. (b) Cheong, S.-W.; Mostovoy, M. *Nat. Mater.* **2007**, *6*, 13. (c) Eerenstein, W.; Mathur, N. D.; Scott, J. F. *Nature* **2006**, *442*, 759. (d) Khomskii, D. I. *J. Magn. Magn. Mater.* **2006**, *306*, 1. (e) Fiebig, M. *J. Phys. D: Appl. Phys.* **2005**, *38*, R123. (f) Hill, N. A. *Annu. Rev. Mater. Res.* **2002**, *32*, 1.
(2) Hill, N. A. *J. Phys. Chem. B* **2000**, *104*, 6694.
(3) Belik, A. A.; Iikubo, S.; Kodama, K.; Igawa, N.; Shamoto, S.; Niitaka, S.; Azuma, M.; Shimakawa, Y.; Takano, M.; Izumi, F.; Takayama-Muromachi, E. *Chem. Mater.* **2006**, *18*, 798.
(4) Baettig, P.; Schelle, C. F.; LeSar, R.; Waghmare, U. V.; Spaldin, N. A. *Chem. Mater.* **2005**, *17*, 1376.
(5) Suchomel, M. R.; Fogg, A. M.; Allix, M.; Niu, H.; Claridge, J. B.; Rosseinsky, M. J. *Chem. Mater.* **2006**, *18*, 4987.
(6) Belik, A. A.; Wuernisha, T.; Kamiyama, T.; Mori, K.; Maie, M.; Nagai, T.; Matsui, Y.; Takayama-Muromachi, E. *Chem. Mater.* **2006**, *18*, 133.
(7) Sugawara, F.; Iiida, S.; Syono, Y.; Akimoto, S. *J. Phys. Soc. Jpn.* **1968**, *25*, 1553.
(8) Moreira dos Santos, A.; Cheetham, A. K.; Atou, T.; Syono, Y.; Yamaguchi, Y.; Ohoyama, K.; Chiba, H.; Rao, C. N. R. *Phys. Rev. B* **2002**, *66*, 064425.
(9) Kimura, T.; Kawamoto, S.; Yamada, I.; Azuma, M.; Takano, M.; Tokura, Y. *Phys. Rev. B* **2003**, *67*, 180401(R).
(10) Niitaka, S.; Azuma, M.; Takano, M.; Nishibori, E.; Takata, M.; Sakata, M. *Solid State Ionics* **2004**, *172*, 557.
(11) Wang, J.; Neaton, J. B.; Zheng, H.; Nagarajan, V.; Ogale, S. B.; Liu, B.; Viehland, D.; Vaithyanathan, V.; Schlom, D. G.; Waghmare, U. V.; Spaldin, N. A.; Rabe, K. M.; Wuttig, M.; Ramesh, R. *Science* **2003**, *299*, 1719.
(12) Ishiwata, S.; Azuma, M.; Takano, M.; Nishibori, E.; Takata, M.; Sakata, M.; Kato, K. *J. Mater. Chem.* **2002**, *12*, 3733.
(13) Yang, C. H.; Koo, T. Y.; Lee, S. H.; Song, C.; Lee, K. B.; Jeong, Y. H. *Europhys. Lett.* **2006**, *74*, 348.
(14) Yang, C. H.; Koo, J.; Song, C.; Koo, T. Y.; Lee, K. B.; Jeong, Y. H. *Phys. Rev. B* **2006**, *73*, 224112.
(15) Atou, T.; Chiba, H.; Ohoyama, K.; Yamaguchi, Y.; Syono, Y. *J. Solid State Chem.* **1999**, *145*, 639.
(16) dos Santos, A. M.; Parashar, S.; Raju, A. R.; Zhao, Y. S.; Cheetham, A. K.; Rao, C. N. R. *Solid State Commun.* **2002**, *122*, 49.
(17) Eerenstein, W.; Morrison, F. D.; Scott, J. F.; Mathur, N. D. *Appl. Phys. Lett.* **2005**, *87*, 101906.

10.1021/cm062772l CCC: $37.00
Published on Web 03/07/2007

$BiMnO_3$ was believed to crystallize in monoclinic space group $C2$ at room temperature (RT).[15] $BiCrO_3$[10] and Bi_2NiMnO_6[18] were reported to be isostructural with $BiMnO_3$, that is, having space group $C2$. Using convergent beam electron diffraction (CBED) and high-resolution neutron powder diffraction, we have shown that the crystal structure of the bulk $BiMnO_3$ can be well-described in the centrosymmetric space group $C2/c$ with lattice parameters of $a = 9.5415$ Å, $b = 5.6126$ Å, $c = 9.8632$ Å, and $\beta = 110.658°$.[19] It was also found that $BiScO_3$ crystallizes in the centrosymmetric space group $C2/c$ and has a crystal structure similar to that of $BiMnO_3$.[20] Quite recently, $BiCrO_3$ was shown to have antiferroelectric properties.[21] This result suggests that $BiCrO_3$ has a centrosymmetric crystal structure.

$BiMnO_3$ undergoes two high-temperature phase transitions at $T_1 = 474$ K and $T_2 = 770$ K.[9,19,22−24] The phase transition at 474 K is a monoclinic-to-monoclinic phase transition without any detectable change in the symmetry[9,19,24] accompanied by a thermal effect,[9,19,22] abrupt changes in lattice parameters and unit-cell volume,[9,24] a small jump in resistivity[9] and magnetization,[19] and an anomaly in the dielectric constant.[22] The low-temperature monoclinic phase (phase I) is characterized by the monoclinic β angle of about 110°, and the high-temperature monoclinic phase (phase II) has a β of about 108°.[9,19,24] The phase transition at 770 K is monoclinic-to-orthorhombic (with space group *Pnma* and lattice parameters of $a = 5.629$ Å, $b = 7.897$ Å, and $c = 5.537$ Å for the orthorhombic phase).[9,24]

In this work, we have investigated the solid solutions of $BiMn_{1-x}Sc_xO_3$ and the effect of nonmagnetic ion substitution on the properties of $BiMnO_3$. The orbital order in $BiMnO_3$ is destroyed by the 5% substitution of Sc for Mn. The temperature of the structural monoclinic-to-orthorhombic phase transition increases with increasing x. The ferromagnetic Curie temperature decreases with increasing Sc content, and long-range magnetic order persists for $x = 0-0.2$. Spin-glass behavior was observed for $x > 0.3$. Using selected area electron diffraction (SAED) and CBED, we have found that $BiMn_{0.9}Sc_{0.1}O_3$ has $C2/c$ symmetry. The crystal structure of $BiMn_{0.9}Sc_{0.1}O_3$ was investigated by the Rietveld method.

2. Experimental Section

2.1. Synthesis. The solid solutions of $BiMn_{1-x}Sc_xO_3$ were prepared for $x = 0$, 0.05, 0.1, 0.2, 0.3, 0.4, 0.5, 0.7, and 1. Stoichiometric mixtures of Bi_2O_3 (99.99%), Sc_2O_3 (99.9%), and Mn_2O_3 were placed in Au capsules and treated at 6 GPa in a belt-type high pressure apparatus at 1383 K ($x = 0$)[19] and 1443 K ($x > 0$) for 60−70 min. After heat treatment, the samples were quenched to RT, and the pressure was slowly released. The resulting samples were black or dark gray powders except for $BiScO_3$, which was white powder. X-ray powder diffraction (XRD) showed that $BiMnO_3$ and $BiScO_3$ were single-phased, and $BiMn_{1-x}Sc_xO_3$ with $0 < x < 1$ contained a small amount of $Bi_2O_2CO_3$ as an impurity. Single-phased Mn_2O_3 was prepared from a commercial MnO_2 (99.99%) by heating in air at 923 K for 24 h. High-resolution neutron powder diffraction studies revealed no detectable changes in stoichiometry of $BiMnO_3$.[19] Because the Au capsules are sealed during synthesis, it is believed that there is no oxygen stoichiometry change.

2.2. Physical Properties. Magnetic susceptibilities, $\chi = \mathbf{M}/\mathbf{H}$, of $BiMn_{1-x}Sc_xO_3$ were measured on a SQUID magnetometer (Quantum Design, MPMS) between 2 and 300 K (2 and 350 K for $BiMnO_3$) in an applied field of 100 Oe under both zero-field-cooled (ZFC) and field-cooled (FC) conditions. Isothermal magnetization measurements were performed between −50 and 50 kOe at 5 K. Specific heat, C_p, at magnetic fields of 0 and 90 kOe was recorded between 2 and 300 K on cooling by a pulse relaxation method using a commercial calorimeter (Quantum Design PPMS). For the specific heat measurements, the powder samples were cold-pressed at 1 GPa to make pellets. Frequency dependent ac susceptibility measurements of $BiMn_{0.6}Sc_{0.4}O_3$ at zero static magnetic field were performed with a Quantum Design MPMS instrument from 60 to 2 K at frequencies (f) of 0.5, 1.99, 7, 25, 99.9, and 299.5 Hz and an applied oscillating magnetic field (H_{ac}) of 5 Oe. We also measured the ac susceptibilities of $BiMn_{0.6}Sc_{0.4}O_3$ at zero static magnetic field and frequency of 110 Hz at different H_{ac} (0.05, 0.1, 0.5, 1, and 5 Oe) from 5 to 60 K.

2.3. Thermal Analysis. Differential scanning calorimetry (DSC) curves of $BiMn_{1-x}Sc_xO_3$ were recorded on a SII Exstar 6000 (DSC 6220) system at a heating/cooling rate of 10 K/min from 133 K to maximum 873 K in semiclosed aluminum capsules. Each sample was heated above ∼30−50 K from the peak position observed above 750 K.

2.4. XRD Experiments and Structure Refinements. XRD data of $BiMn_{1-x}Sc_xO_3$ and $BiMn_{0.9}Sc_{0.1}O_3$ were collected at RT on a RIGAKU Ultima III diffractometer using CuK_α radiation (2θ range of 8−110°, a step width of 0.02°, and a counting time of 9 s/step for $BiMn_{0.9}Sc_{0.1}O_3$, and 2θ range of 8−80°, a step width of 0.02°, and a counting time of 2 s/step for all other samples). The XRD data were analyzed by the Rietveld method with RIETAN-2000.[25] Coefficients for analytical approximation to atomic scattering factors for Bi, Mn, Sc, and O were taken from ref 26. The pseudo-Voigt function of Toraya was used as a profile function.[27] The background was represented by a seventh-order Legendre polynomial. Isotropic atomic displacement parameters, B, with the isotropic Debye−Waller factor represented as $\exp((-B \sin^2\theta)/\lambda^2)$ were assigned to all the sites. For the impurity of $Bi_2O_2CO_3$, we refined only a scale factor and the lattice parameters, fixing its structure parameters. The mass percentage of $Bi_2O_2CO_3$ in $BiMn_{0.9}Sc_{0.1}O_3$ was calculated at 0.8% from the refined scale factors. Note that the amount of $Bi_2O_2CO_3$ in other $BiMn_{1-x}Sc_xO_3$ samples did not exceed 1%.

2.5. SAED and CBED Studies. The bulk $BiMn_{0.9}Sc_{0.1}O_3$ specimen was crushed and dispersed on a carbon thin film on a Cu grid for transmission electron microscopy. The SAED and CBED patterns were taken at 300 K using an analytical transmission

(18) Azuma, M.; Takata, K.; Saito, T.; Ishiwata, S.; Shimakawa, Y.; Takano, M. *J. Am. Chem. Soc.* **2005**, *127*, 8889.
(19) Belik, A. A.; Iikubo, S.; Yokosawa, T.; Kodama, K.; Igawa, N.; Shamoto, S.; Azuma, M.; Takano, M.; Kimoto, K.; Matsui, Y.; Takayama-Muromachi, E. *J. Am. Chem. Soc.* **2007**, *129*, 971−974.
(20) Belik, A. A.; Iikubo, S.; Kodama, K.; Igawa, N.; Shamoto, S.; Maie, M.; Nagai, T.; Matsui, Y.; Stefanovich, S. Yu.; Lazoryak, B. I.; Takayama-Muromachi, E. *J. Am. Chem. Soc.* **2006**, *128*, 706.
(21) Kim, D. H.; Lee, H. N.; Varela, M.; Christen, H. M. *Appl. Phys. Lett.* **2006**, *89*, 162904.
(22) Chi, Z. H.; Xiao, C. J.; Feng, S. M.; Li, F. Y.; Jin, C. Q.; Wang, X. H.; Chen, R. Z.; Li, L. T. *J. Appl. Phys.* **2005**, *98*, 103519.
(23) Montanari, E.; Righi, L.; Calestani, G.; Migliori, A.; Gilioli, E.; Bolzoni, F. *Chem. Mater.* **2005**, *17*, 1765.
(24) Montanari, E.; Calestani, G.; Migliori, A.; Dapiaggi, M.; Bolzoni, F.; Cabassi, R.; Gilioli, E. *Chem. Mater.* **2005**, *17*, 6457.
(25) Izumi, F.; Ikeda, T. *Mater. Sci. Forum* **2000**, *321−324*, 198.
(26) *International Tables for Crystallography*, 2nd ed.; Wilson, A. J. C., Prince, E., Eds.; Kluwer: Dordrecht, The Netherlands, 1999; Vol. C, pp 572−574.
(27) Toraya, H. *J. Appl. Crystallogr.* **1990**, *23*, 485.

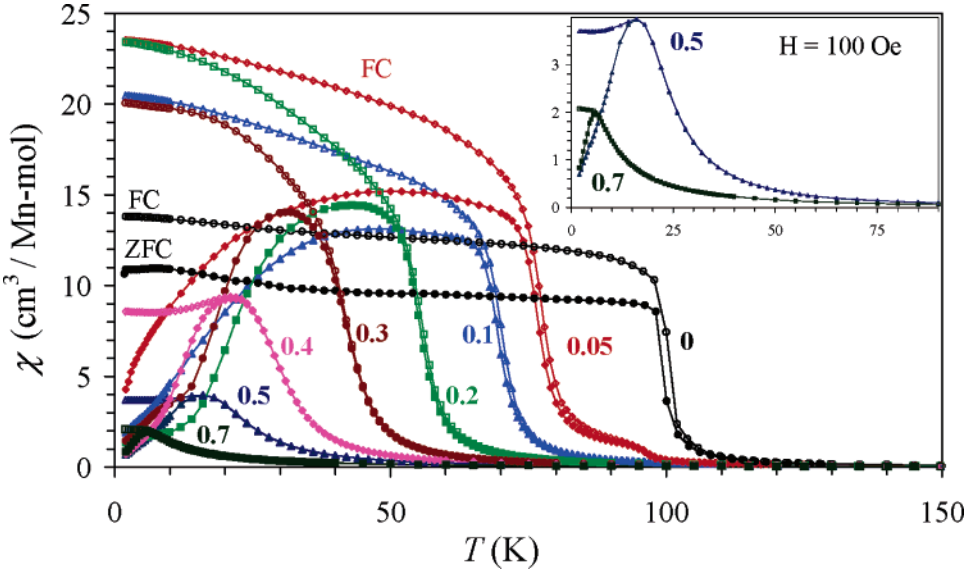

Figure 1. ZFC (full symbols) and FC (empty symbols) magnetic susceptibility ($\chi = \mathbf{M/H}$) curves of $BiMn_{1-x}Sc_xO_3$ measured at 100 Oe. The inset gives the enlarged curves for $x = 0.5$ and 0.7.

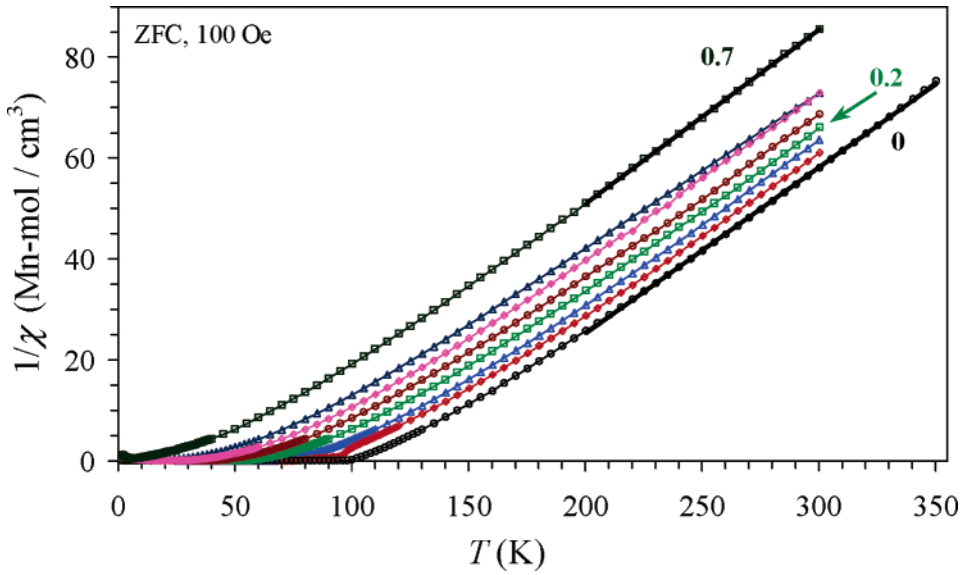

Figure 2. Inverse ZFC curves (symbols with lines) of $BiMn_{1-x}Sc_xO_3$ with the Curie−Weiss fits (bold lines).

electron microscope (Hitachi: HF-3000S) with a cold field-emission gun operated at an accelerating voltage of 300 kV. The SAED and CBED patterns were taken from specimen areas of about 300 and 10 nm in diameter, respectively.

3. Results

3.1. Physical and Chemical Properties of $BiMn_{1-x}Sc_xO_3$. Figure 1 shows magnetic susceptibilities of $BiMn_{1-x}Sc_xO_3$. A pronounced irreversibility is observed between the ZFC and FC curves for all the compositions below a certain temperature. In addition, there is a temperate hysteresis in the region of the strong upturn of susceptibilities for the compositions with $0 \le x \le 0.3$, whereas no such hysteresis is observed for $x \ge 0.4$. The FC χ vs T curve of $BiMn_{0.95}Sc_{0.05}O_3$ exhibits the first steplike increase near 97 K and then a second main increase below 78 K. The FC χ vs T curves of other samples show a one-step transition. The FC χ vs T curves of the samples with $0 \le x \le 0.3$ increase monotonically at low temperatures, whereas the FC χ vs T curves of the samples with $x = 0.4$ and 0.5 demonstrate a broad maximum and are almost constant at lower temperatures. The FC χ vs T curve of $BiMn_{0.3}Sc_{0.7}O_3$ differs from those of $BiMn_{0.6}Sc_{0.4}O_3$ and $BiMn_{0.5}Sc_{0.5}O_3$ by the absence of a broad maximum. Another feature of the magnetization data is that the ZFC curves of the undoped $BiMnO_3$ and $BiMn_{1-x}Sc_xO_3$ are quite different. In $BiMnO_3$, the ZFC curve measured at low magnetic fields shows a small hump at low temperatures, and then it is almost constant in a wide temperature range below T_M (Figure 1 and ref 23). This behavior is typical for a ferromagnet. In $BiMn_{1-x}Sc_xO_3$ with $x \ge 0.05$, the ZFC curves demonstrate very broad maxima typical for cluster-glass-like or spin-glass-like materials.

The inverse ZFC magnetic susceptibilities (Figure 2) between 200 and 300 K are fit by the Curie−Weiss equation

$$\chi(T) = \mu^2_{\text{eff}} N(3k_B(T-\theta))^{-1} \quad (1)$$

where μ_{eff} is an effective magnetic moment, N is Avogadro's

Table 1. Different Parameters Deduced from the Magnetization Curves of $BiMn_{1-x}Sc_xO_3$[a]

x	μ_{eff} (μ_B)	θ (K)	T_M (K)	H_c (Oe)	M_r (μ_B)	M_S (μ_B)
0	4.93	123	102.0	~3	0.013	3.92
0.05	4.97	112	96.9, 77.9	~70	0.271	3.76
0.1	4.94	107	70.0	~150	0.428	3.71
0.2	4.99	96	56.1	~630	0.975	3.51
0.3	4.97	89	42	~600	1.023	3.31
0.4	4.90	82	30	~520	0.430	3.01
0.5	5.10	63	22	~300	0.159	2.78
0.7	4.82	52	8	0	0	2.58

[a] T_M is defined by the peak position on the FC $d\chi/dT$ vs T curves (see the Supporting Information). H_c is the coercive field at 5 K, M_r is the remnant magnetization at 5 K, and M_S is the magnetization at 5 K and 50 kOe. All the values are given per mol of Mn^{3+} ions or per a Mn^{3+} ion.

number, k_B is Boltzmann's constant, and θ is the Weiss constant. The fitted parameters are summarized in Table 1. The effective magnetic moment for all the samples is close to the localized Mn^{3+} moment of $4.90\mu_B$. For all the compositions, the FC $d\chi/dT$ vs T curves demonstrate peaks whose width increases and intensity decreases with increasing x (see the Supporting Information). The position of the peaks defining T_M are given in Table 1. The sample with $x = 0.05$ clearly shows two anomalies on the $d\chi/dT$ vs T curve at $T_M = 96.9$ and 77.9 K.

Figure 3 depicts the isothermal magnetization curves at 5 K. The coercive field (H_c) and the remnant magnetization (M_r) increase with increasing the content of Sc up to $x = 0.2$. Then the H_c and M_r decrease for $x > 0.2$, and the H_c and M_r cannot be detected for $x = 0.7$. The H_c and M_r values and the magnetic moment at 5 K and 50 kOe (M_S) are reported in Table 1. The M_S is about $3.92\mu_B$ per Mn^{3+} in $BiMnO_3$ and decreases in $BiMn_{1-x}Sc_xO_3$ with increasing x. Note that the first magnetization curves from 0 to 50 kOe are not inside the hysteresis loops but slightly lower than the curves measured from 50 to −50 kOe and from −50 to 50 kOe (see the Supporting Information).

Figure 4 gives the real ($\chi' = \mathbf{M}'/\mathbf{H}_{ac}$) and imaginary ($\chi'' = \mathbf{M}''\mathbf{H}_{ac}$) parts of the ac susceptibilities of $BiMn_{0.6}Sc_{0.4}O_3$ at zero static magnetic field between 2 and 60 K measured at different frequencies. Both curves exhibit evident maxima with intensities and positions depending on frequency. The peak intensity of χ' vs T is suppressed and the peak position is shifted to higher temperatures with increasing frequency. The peak intensity of χ'' vs T increases and the peak position is shifted to higher temperatures with increasing frequency. Note that the maxima on the χ' vs T and χ'' vs T curves occur at slightly different temperatures. These features are reminiscent of the spin-glass behavior.[29] In spin glasses, a criterion, $\delta T_f = \Delta T_f/(T_f \Delta \log f)$, has often been used for comparing the frequency dependence of the spin freezing temperature T_f. With the values $T_f = 23.88(4)$ K at $f = 0.5$ Hz and $T_f = 24.65(3)$ K at $f = 299.5$ Hz, we obtain $\delta T_f = 0.0116$. This value is comparable with those reported for some spin glasses ($\delta T_f = 0.001-0.01$).[29] We assumed the variation of χ' to a Gaussian function near T_f to determine T_f. Note that T_M and T_f are different for $BiMn_{0.6}Sc_{0.4}O_3$. In some cases, it is difficult to distinguish between spin glasses, re-entrant spin-glasses, superparamagnets, and ferromagnets. In spin glasses, the ac field interacts with randomly oriented separate moments. In ferromagnets, the ac field interacts with ferromagnetic domain walls. Therefore, spin glasses and ferromagnets have different dependence of the ac susceptibilities on the frequency and H_{ac}.[30] We did not observe any dependence of the real part of the ac susceptibilities of $BiMn_{0.6}Sc_{0.4}O_3$ on H_{ac} between $H_{ac} = 0.05$ and 5 Oe (see the Supporting Information). The above results give strong support that a spin-glass transition takes place in $BiMn_{0.6}Sc_{0.4}O_3$.

Figure 5 shows the specific heat of $BiMn_{1-x}Sc_xO_3$ plotted as C_p/T vs T. The λ-type anomaly on the C_p vs T curve of $BiMnO_3$ is observed at 97.5 K in agreement with the previous measurements.[9,31] The anomaly near T_M is strongly suppressed for $x > 0$. A very small anomaly near T_M is still observed for $x = 0.2$, but no anomaly is found for $x = 0.3$. Two anomalies are seen in $BiMn_{0.95}Sc_{0.05}O_3$ on the C_p/T vs T curve in agreement with the magnetic susceptibility data. Another feature of the specific heat data is the strong increase of the magnetic contribution at low temperatures with increasing the x value (Figure 5b). The measurements in the magnetic field of 90 kOe for $BiMnO_3$[31] and $BiMn_{0.5}Sc_{0.5}O_3$ (see the Supporting Information) showed a decrease in the specific heat in a wide temperature range and smearing the ferromagnetic transition.

The DSC curves of $BiMn_{1-x}Sc_xO_3$ are given in Figure 6. $BiMnO_3$ demonstrates two clear peaks at 474 and 768 K (on heating).[19,22] The cycling of the DSC curves of $BiMnO_3$ between 300 and 520 K gives reproducible results without any change in the peak position and intensity. However, after $BiMnO_3$ was heated to 790 K, the phase transition near 474 K was smeared during the cooling measurement. And the subsequent cycling of the DSC curves between 300 and 520 K showed the shift in the monoclinic-to-monoclinic phase transition to 469 K (see the Supporting Information). The phase transition in $BiMnO_3$ near 474 K disappears on doping 5% of Sc^{3+} ions. This phase transition is not detected in $BiMn_{0.95}Sc_{0.05}O_3$ down to 133 K. The temperature corresponding to the monoclinic-to-orthorhombic phase transition increases with increasing Sc content. All the high-temperature transitions in $BiMn_{1-x}Sc_xO_3$ show the temperature hysteresis. The hysteresis width (and also the temperature of heating) increases with increasing the Sc content. This fact can be explained by the partial decomposition or oxygen-content changes during heating to 800−873 K in air. The partial/complete decomposition of $BiMnO_3$ after heating at 800/873 K was reported in the literature.[24,32] The XRD data of $BiMn_{1-x}Sc_xO_3$ collected after the DSC experiments showed that the reflections were noticeably broader compared with those of the as-prepared samples (see the Supporting Information).

(28) Belik, A. A.; Takayama-Muromachi, E. Unpublished results.
(29) J. A. Mydosh, *Spin Glass: An Experimental Introduction*; Taylor & Francis: London, 1993.
(30) Coronado, E.; Gomez-Garcia, C. J.; Nuez, A.; Romero, F. M.; Waerenborgh, J. C. *Chem. Mater.* **2006**, *18*, 2670 and references therein.
(31) Belik, A. A.; Takayama-Muromachi, E. *Inorg. Chem.* **2006**, *45*, 10224.
(32) Faqir, H.; Chiba, H.; Kikuchi, M.; Syono, Y.; Mansori, M.; Satre, P.; Sebaoun, A. *J. Solid State Chem.* **1999**, *142*, 113.

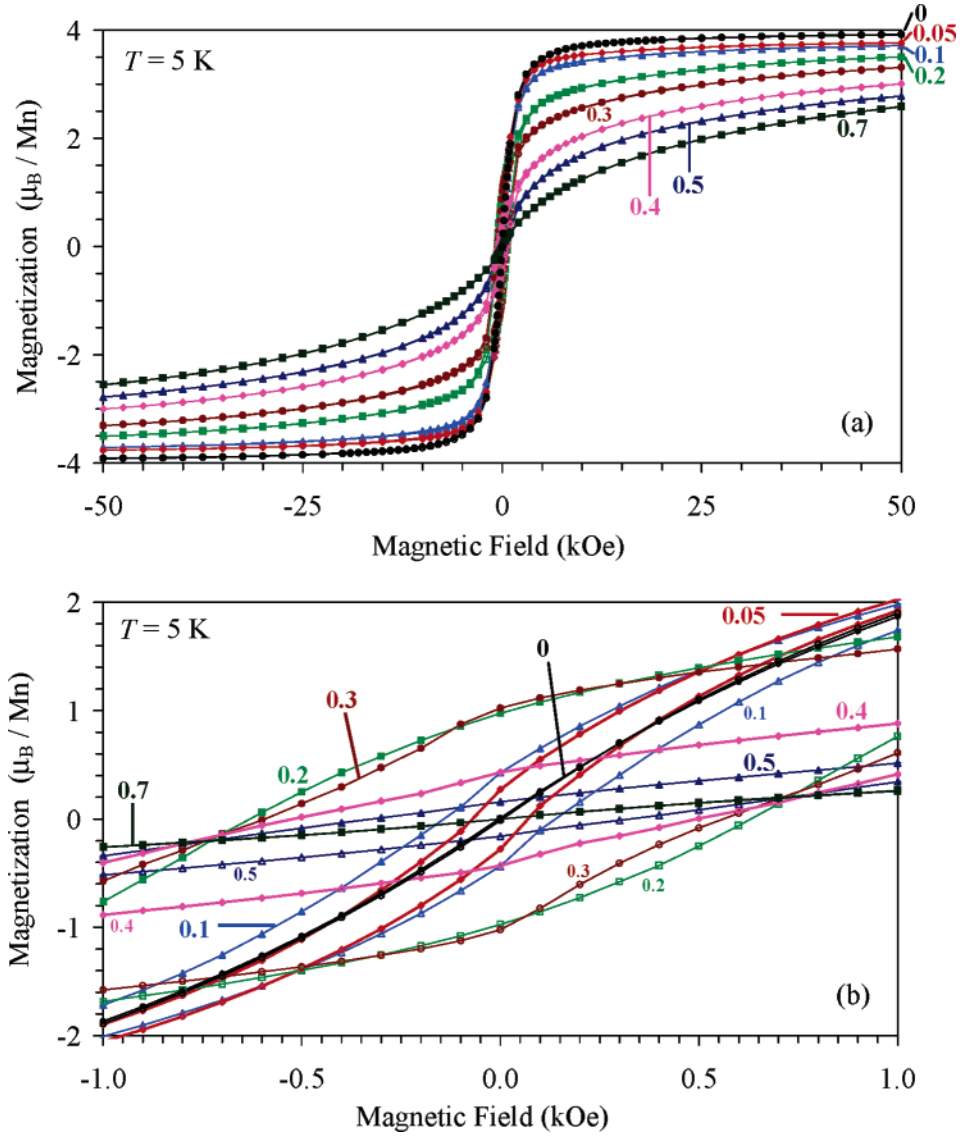

Figure 3. (a) Isothermal magnetization curves of $BiMn_{1-x}Sc_xO_3$ at 5 K. (b) Enlarged isothermal magnetization curves at 5 K between −1 and 1 kOe.

3.2. Structural Properties of $BiMn_{1-x}Sc_xO_3$ and $BiMn_{0.9}Sc_{0.1}O_3$. Indexing Bragg reflections in the XRD patterns of $BiMn_{1-x}Sc_xO_3$ reveal them to crystallize in the monoclinic system. Reflection conditions derived from the indexed reflections were $h + k = 2n$ for hkl, and $h = 2n$ and $l = 2n$ for $h0l$, affording possible space groups Cc (No. 9) and $C2/c$ (No. 15) similar to $BiScO_3$.[20] The lattice parameters are refined by the Rietveld method adopting the $C2/c$ model (see below) and summarized in Table 2. The dependence of the lattice parameters on composition is given in Figure 7.The reflection conditions of $BiMn_{0.9}Sc_{0.1}O_3$ are checked and confirmed using SAED (Figure 8). Reflections with $l = 2n+1$ for $00l$ observed on the [100] zone axis are due to the double diffraction because no such reflections are found on the [010] zone axis. To distinguish between $C2/c$ and Cc, we use the CBED technique. The symmetry of CBED patterns including higher-order Laue zone (HOLZ) reflections yields information on three-dimensional symmetry elements of the crystal structure around the zone axis parallel to the incident beam direction. Figure 9 shows the [100] CBED pattern. The ring-shaped reflections around the center of the CBED pattern indicated by arrows stem from HOLZ. The HOLZ reflections in the CBED pattern clearly show the mirror-plane symmetry perpendicular to the *b*-axis. We also confirm the 2-fold rotational symmetry along the *b*-axis by CBED. Therefore, $BiMn_{0.9}Sc_{0.1}O_3$ belongs to a point group $2/m$. In addition, we observe the dynamical extinction rule (GM-line) for the $00l$ reflections with $l = 2n + 1$ on the [100] CBED zero-order Laue zone (ZOLZ) pattern (Figure 8c). This result shows that there is a *c*-glide plane perpendicular to the *b*-axis. All the above results give the centrosymmetric space group $C2/c$ for $BiMn_{0.9}Sc_{0.1}O_3$.

For starting fractional coordinates in Rietveld analysis of $BiMn_{0.9}Sc_{0.1}O_3$, we used those of $BiScO_3$ with space group $C2/c$.[20] In the structure analysis, the *B* parameters for the O atoms were constrained to be the same ($B(O1) = B(O2) = B(O3)$). Final lattice parameters, *R* factors, fractional coordinates, and *B* parameters are listed in Table 3, and selected bond lengths and angles calculated with ORFFE[33] in Table 4. Figure 10 displays observed, calculated, and difference XRD patterns.

(33) Busing, W. R.; Martin, K. O.; Levy H. A. *Report ORNL-TM-306*; Oak Ridge National Laboratory: Oak Ridge, TN, 1964.

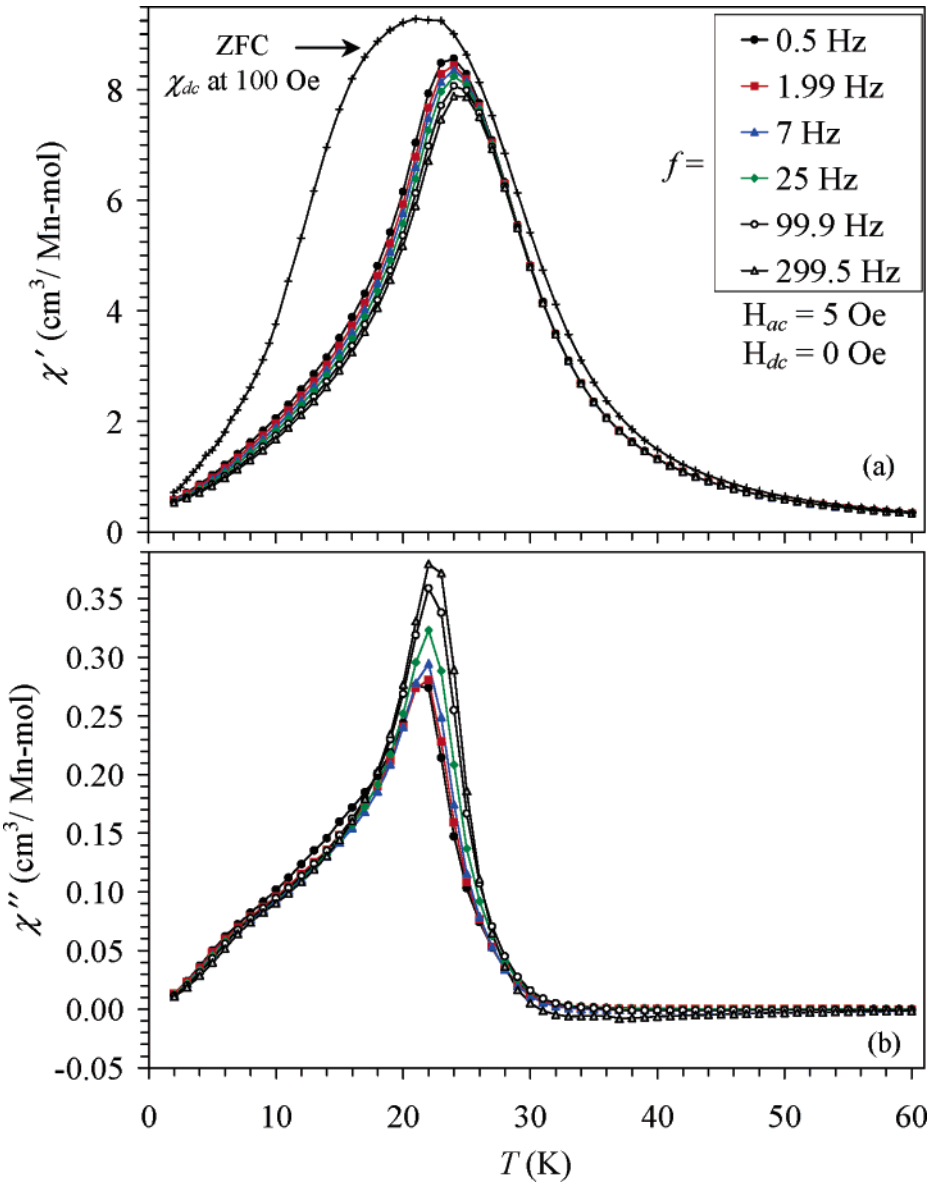

Figure 4. Frequency dependence of (a) the real χ' and (b) imaginary χ'' parts of the ac susceptibilities of $BiMn_{0.6}Sc_{0.4}O_3$ measured on cooling from 60 K at zero static magnetic field and an applied oscillating magnetic field (H_{ac}) of 5 Oe. The ZFC χ vs T curve is given for the comparison.

4. Discussion

The CBED results showed that $BiMn_{0.9}Sc_{0.1}O_3$ crystallizes in the centrosymmetric space group $C2/c$ similar to the end member $BiScO_3$.[20] The analysis of the Mn−O bond lengths suggests that there is no orbital ordering in $BiMn_{0.9}Sc_{0.1}O_3$ at RT compared with $BiMnO_3$ at RT. The Mn−O interatomic distances and lattice parameters are close in $BiMn_{0.9}Sc_{0.1}O_3$ at RT and in $BiMnO_3$ at 550 K (Tables 2 and 4) indicating that the high-temperature monoclinic phase II of $BiMnO_3$ (above 474 K) is the same as $BiMn_{0.9}Sc_{0.1}O_3$. From the β values, one can conclude that the $BiMn_{1-x}Sc_xO_3$ samples with $x \geq 0.05$ adopt the monoclinic phase II structure. The lattice parameters of $BiMn_{1-x}Sc_xO_3$ with $x \geq 0.05$ show monotonic changes with changing the composition. However, in $BiMnO_3$, the lattice parameters demonstrate sudden jumps. The origin of these jumps is believed to be the appearance of the cooperative static Jahn−Teller distortion in the monoclinic phase I of $BiMnO_3$ and orbital order. By the extrapolation one can obtain the lattice parameters of $BiMnO_3$, which it would have at RT without the orbital order.

All the compositions $BiMn_{1-x}Sc_xO_3$ have a positive Weiss constant (Table 1). This fact shows that the interaction between Mn^{3+} ions is predominantly ferromagnetic even in the highly diluted samples where the long range orbital and spin orders cannot take place at all the temperatures. This ferromagnetic interaction can be explained by the local distortions and the dynamic Jahn−Teller effect.[34,35] The Weiss constant monotonically decreases with increasing x, suggesting a decrease in the ferromagnetic correlations. The observation of the anomalies on the specific heat near T_M for the samples with $x = 0.05-0.2$ shows that long-range magnetic order may take place in these samples. However, the specific heat anomalies of the samples with $x = 0.05-$

(34) Zhou, J. S.; Goodenough, J. B. *Phys. Rev. B* **2003**, *68*, 144406.
(35) Zhou, J. S.; Yin, H. Q.; Goodenough, J. B. *Phys. Rev. B* **2001**, *63*, 184423.

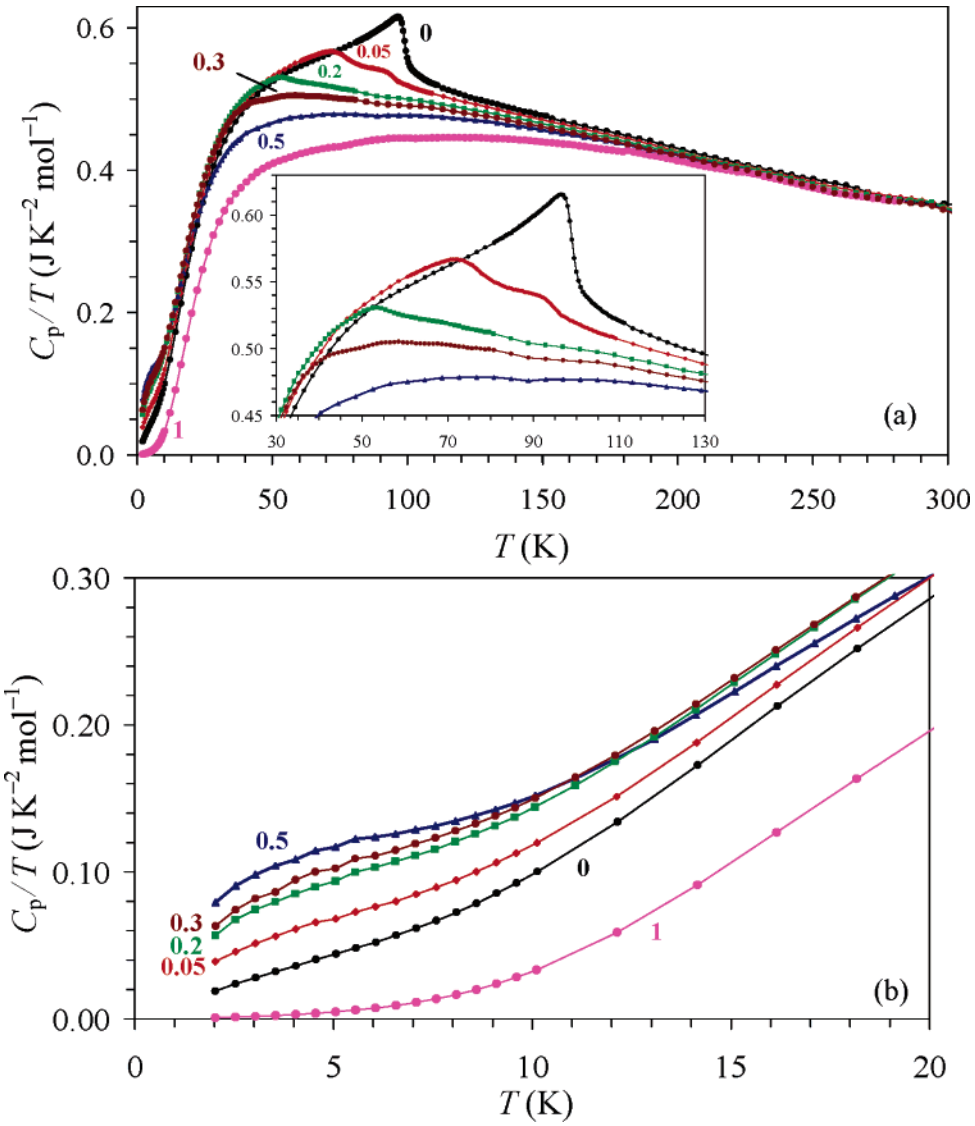

Figure 5. (a) C_p/T vs T curves of $BiMn_{1-x}Sc_xO_3$ between 2 and 300 K at zero magnetic field. The inset shows a fragment near the phase-transition temperatures. Data for $x = 0$ and 1 are from ref 31. (b) C_p/T vs T curves of $BiMn_{1-x}Sc_xO_3$ at the low-temperature region between 2 and 20 K.

0.2 are significantly smeared compared with that of $BiMnO_3$. This fact and the characteristic ZFC curves may suggest the formation of ferromagnetic clusters (with long-range order) that become smaller with increasing Sc content. In $BiMn_{0.6}Sc_{0.4}O_3$, the ac susceptibility measurements confirm the appearance of a spin-glass state (Figure 4). Note that spin-glass features were observed in the undoped $BiMnO_3$.[13,31] It was suggested that the magnetic specific heat of $BiMnO_3$ has two contributions at low temperatures, one from the ferromagnetic spin waves and another from spin-glass-like states.[31] The spin wave contribution should be suppressed with increasing Sc content. Therefore, low-temperature specific heat data show that cluster-glass and spin-glass contributions are strongly enhanced by increasing Sc content in $BiMn_{1-x}Sc_xO_3$. Spin-glass phases and magnetic-field-induced spin-glass to ferromagnetic transitions were observed in $LaMn_{1-x}M_xO_3$ (M = Sc[36] and Ga[34,35]) near $x = 0.5$. It should be noted that neutron powder diffraction studies have found that a long-range ferromagnetic order is still present in rather diluted samples with $x = 0.5$ and 0.6 in the $LaMn_{1-x}Ga_xO_3$ system.[37] The M vs H curve of $BiMn_{0.3}Sc_{0.7}O_3$ shows no hysteresis ($H_c = 0$ Oe and $M_r = 0\mu_B$) compared with other $BiMn_{1-x}Sc_xO_3$ samples. The similar behavoir in the $LaMn_{1-x}Ga_xO_3$ system for $x = 0.8$ and 0.9 and the absence of magnetic reflections was explained by the formation of a superparamagnetic state.[37] However, the anhysteresis behavoir may be explained by the fact that the transition temperatures of $BiMn_{0.3}Sc_{0.7}O_3$ ($T_M = 8$ K) and $LaMn_{0.2}Ga_{0.8}O_3$ ($T_M = 5.4$ K)[37] are very close to the measurement temperature of the M vs H curves (5 K).

From the above discussion, we can suggest the following evolution of magnetic ground states for the $BiMn_{1-x}Sc_xO_3$ series (Figure 11). $BiMnO_3$ ($x = 0$) has a ferromagnetic (FM) ground state.[8] For $0.05 \le x \le 0.2$, a ferromagnetic cluster-glass (FCG) state is realized that transforms to a spin-glass (SG) state with further dilution of the Mn sublattice for $x \ge 0.4$. In the intermediate region ($x = 0.3$), the change of the

(36) Goodenough, J. B.; Dass, R. I.; Zhou, J. S. *Solid State Sci.* **2002**, *4*, 297.

(37) Blasco, J.; Garcia, J.; Campo, J.; Sanchez, M. C.; Subias, G. *Phys. Rev. B* **2002**, *66*, 174431.

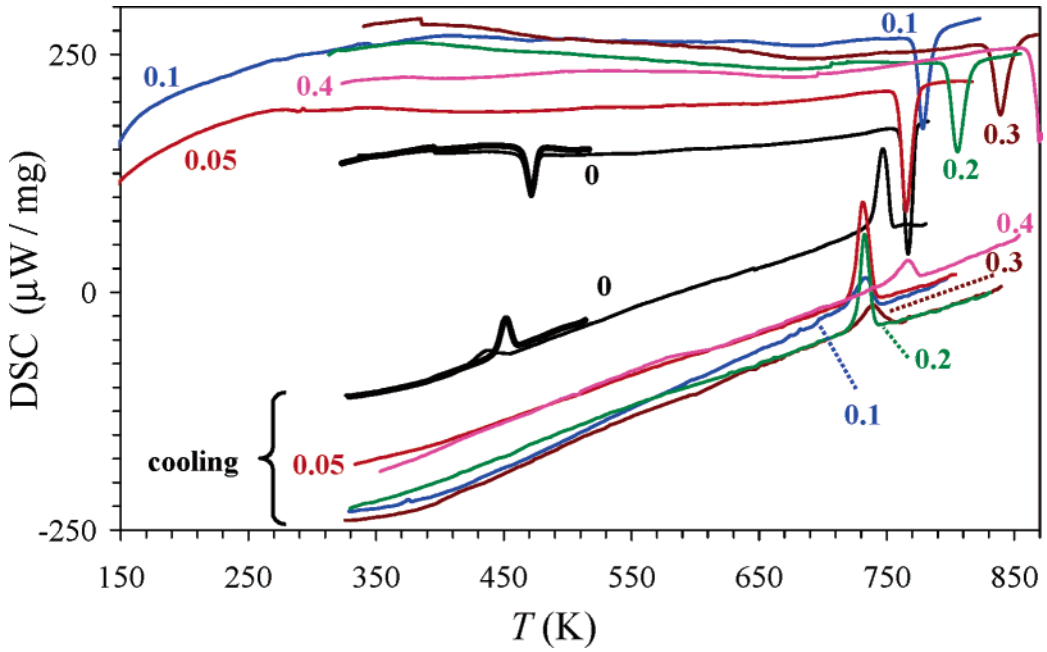

Figure 6. DSC curves of $BiMn_{1-x}Sc_xO_3$. The bold lines for $BiMnO_3$ show the curves cycled between 300 and 520 K. All other curves were measured above 750 K.

Table 2. Lattice Parameters of $BiMn_{1-x}Sc_xO_3$[a]

x	a (Å)	b (Å)	c (Å)	β (deg)	V (Å^3)
0[19]	**9.5415**	**5.61263**	**9.8632**	**110.658**	**494.24**
0.05, Fe[b]	**9.5355**	**5.6103**	**9.8530**	**110.474**	**493.81**
0 (550 K)[19]	9.5866	5.59903	9.7427	108.601	495.63
0.05	9.5850	5.5973	9.7610	108.899	495.45
0.1	9.6029	5.60988	9.7690	108.775	498.26
0.2	9.6227	5.6357	9.7896	108.615	503.12
0.3	9.6458	5.6651	9.8209	108.518	508.88
0.4	9.6719	5.6912	9.8512	108.452	514.38
0.5	9.7010	5.7156	9.8817	108.431	519.81
0.7	9.7714	5.7592	9.9475	108.395	531.19
1[20]	9.8899	5.8221	10.0462	108.300	549.20

[a] At room-temperature if not specified. The bold font shows the compositions in the orbitally ordered state. [b] For $BiMn_{0.95}Fe_{0.05}O_3$.[28]

ground state is possible depending on the temperature. Detailed magnetic investigations including neutron diffraction and ac susceptibility measurements will be needed to confirm the suggested ground states and phase transition sequences.

Careful analysis of the XRD pattern of $BiMn_{0.95}Sc_{0.05}O_3$ revealed that there are two monoclinic phases indicating the phase separation to Sc-poor ($x = 0.05 - \delta_1$; phase I) and Sc-rich phases ($x = 0.05 + \delta_2$; phase II) (see the Supporting Information). The XRD pattern of $BiMn_{0.95}Sc_{0.05}O_3$ was analyzed by the Rietveld method, where the lattice parameters of the Sc-poor phase were fixed at those of $BiMnO_3$ (at RT). The mass percentage of the Sc-poor phase in $BiMn_{0.95}Sc_{0.05}O_3$ was calculated at 3% from the refined scale factors. Note that because of the small amount of the Sc-poor phase, it is impossible to refine its lattice parameters. In addition, all the main reflections of phases I and II overlap with each other. The phase separation explains why two magnetic transitions were observed in $BiMn_{0.95}Sc_{0.05}O_3$. Despite the fact that the amount of the Sc-poor phase is very small, this phase could be detected by specific heat measurements, probably because the specific heat anomaly at T_M in $BiMnO_3$ is rather strong. The fact that T_M of the Sc-poor phase (96.9 K) is slightly smaller than that of $BiMnO_3$ (102.0 K) shows that the Sc-poor phase indeed contains some Sc atoms, and it is not the pure $BiMnO_3$ phase. The sudden decrease in T_M in the Sc-rich phase (77.9 K) and in other $BiMn_{1-x}Sc_xO_3$ samples with $0.1 \leq x \leq 0.7$ having the monoclinic phase II structure (Table 1) gives support that orbital order enhances the magnetic interactions in $BiMnO_3$ and increases T_M.

It should be noted that a two-step magnetic transition was also found in $BiMnO_3$ with a very small upturn near 114 K and the main transition at 99 K.[23,31] The anomaly at 114 K was explained by the presence of a small amount of another perovskite-like modification of $BiMnO_3$.[23] This modification was detected by electron diffraction on the grain boundaries. It could not be detected by powder diffraction methods because of a very small amount and because its reflections seem to overlap with the reflections of the main phase. However, other electron diffraction observations could not detect this minor phase in the as-prepared samples.[38] Its appearance was explained by the effect of electron beam irradiation.

$BiMnO_3$ behaves as a very soft ferromagnet. The introduction of nonmagnetic ions strongly increases the M_r and H_c values as we have found in $BiMn_{1-x}Sc_xO_3$ (Table 1). We can assume that the presence of different defects and nonstoichiometry can also increase the M_r and H_c. This assumption can explain why the M_r and H_c values are quite different between our bulk $BiMnO_3$ sample ($H_c \approx 3$ Oe and $M_r \approx 0.013\mu_B$) and the literature data (e.g., $H_c \approx 200-470$ Oe and $M_r \approx 0.2\mu_B$ for bulk samples[9,16,22] and $H_c \approx 400-1000$ Oe and $M_r \approx 0.5-1.0\mu_B$ for thin film samples).[13,17,39] Because most of the previous works were done on samples containing different impurities, the tiny changes in stoichiometry were

(38) Chi, Z.; Yang, H.; Li, F.; Yu, R.; Jin, C.; Wang, X.; Deng, X.; Li, L. *J. Phys.: Condens. Matter* **2006**, *18*, 4371.
(39) dos Santos, A. F. M.; Cheetham, A. K.; Tian, W.; Pan, X. Q.; Jia, Y. F.; Murphy, N. J.; Lettieri, J.; Schlom, D. G. *Appl. Phys. Lett.* **2004**, *84*, 91.

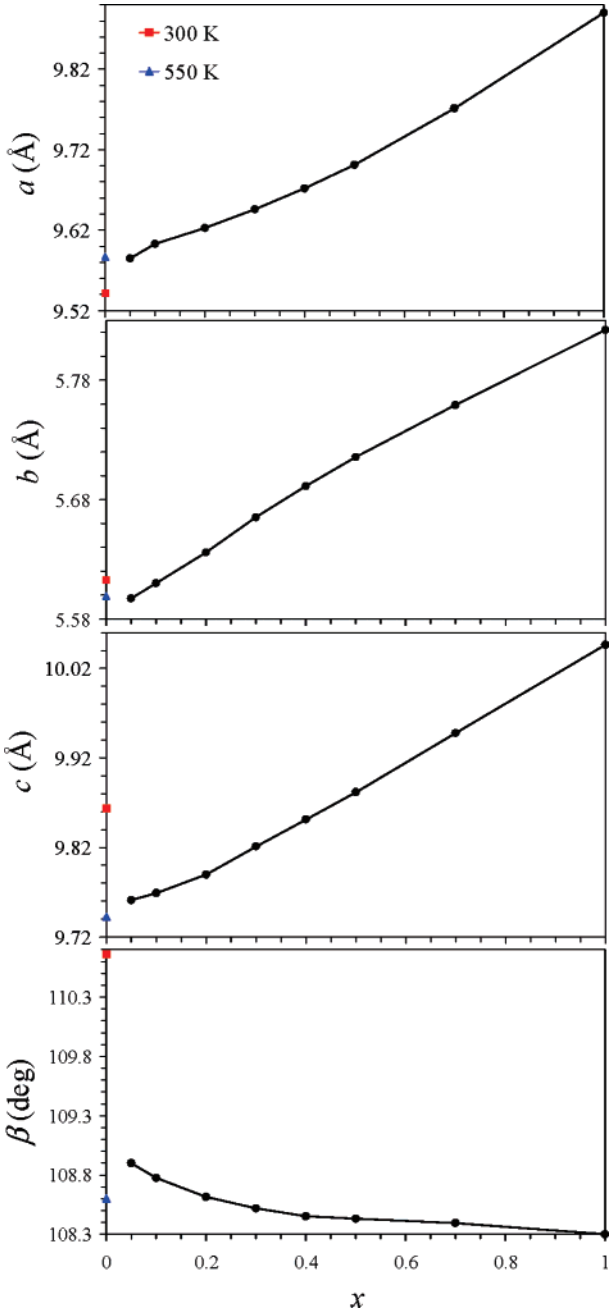

Figure 7. Dependence of the lattice parameters of $BiMn_{1-x}Sc_xO_3$ on the composition. For $BiMnO_3$, the lattice parameters at 300 and 550 K (from ref 19) are given.

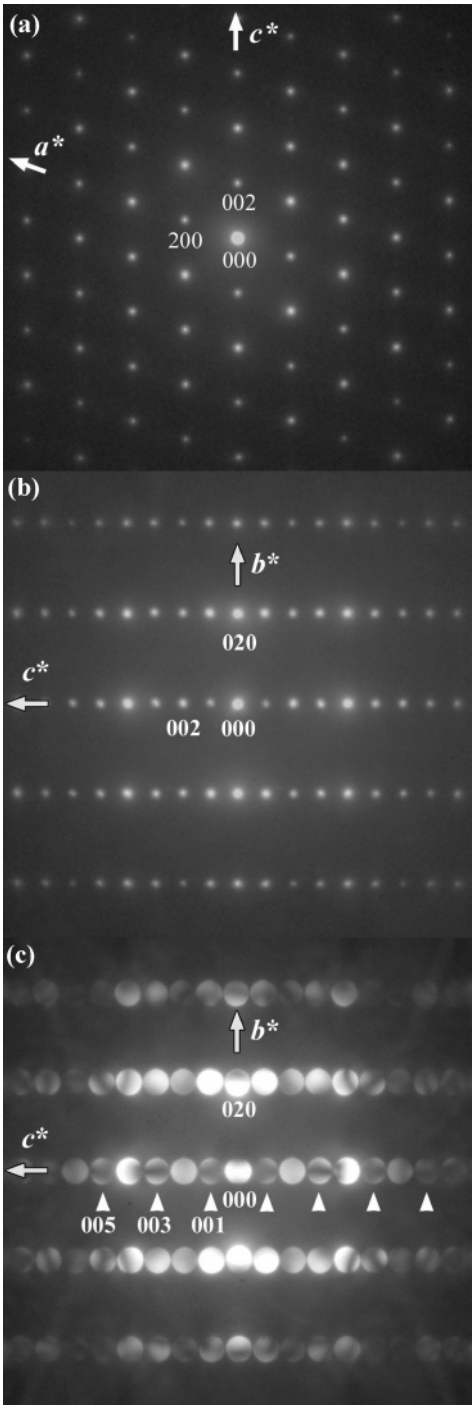

Figure 8. SAED patterns of $BiMn_{0.9}Sc_{0.1}O_3$ taken along the (a) [010] and (b) [100] zone axes. The presence of the 00*l* reflections with $l = 2n + 1$ on the [100] zone axis is due to the double diffraction because these reflections are absent on the [010] zone axis. (c) CBED zero-order Laue zone pattern of $BiMn_{0.9}Sc_{0.1}O_3$ taken along the [100] zone axis. The dynamic extinction rule (GM-line) for the 00*l* ($l = 2n + 1$) reflections is seen, indicating the existence of a *c*-glide plane perpendicular to the *b*-axis.

possible. In ref 24, it was suggested that the thin-film samples in reality consisted of partially oxidized phases because some of these samples showed much lower ferromagnetic transition temperatures. The Bi-deficiency was found in thin-film samples by Rutherford backscattering spectroscopy,[40] and oxygen non-stoichiometry was suggested to explain large conductivity.[39] In thin films, there are additional compressive strains.

The peaks above 750 K on the DSC curves correspond to the monoclinic-to-orthorhombic structural phase transition. The temperature of this transition increases with increasing Sc content. The anomaly observed at 474 K in $BiMnO_3$ corresponds to the monoclinic-to-monoclinic phase transition and is associated with the melting of orbital order in $BiMnO_3$.[19] The 5% substitution of Sc for Mn in $BiMnO_3$ destroys this transition. This fact gives strong support that the transition at 474 K in the undoped $BiMnO_3$ involves the orbital degrees of freedom and corresponds to the orbital melting.

In ref 14, in which the researchers used resonant X-ray scattering, it was proposed that the orbital order in $BiMnO_3$

(40) Sharan, A.; An, I.; Chen, C.; Collins, R. W.; Lettieri, J.; Jia, Y. F.; Schlom, D. G.; Gopalan, V. *Appl. Phys. Lett.* **2003**, *83*, 5169.
(41) Brese, R. E.; O'Keeffe, M. *Acta Crystallogr., Sect. B* **1991**, *47*, 192.

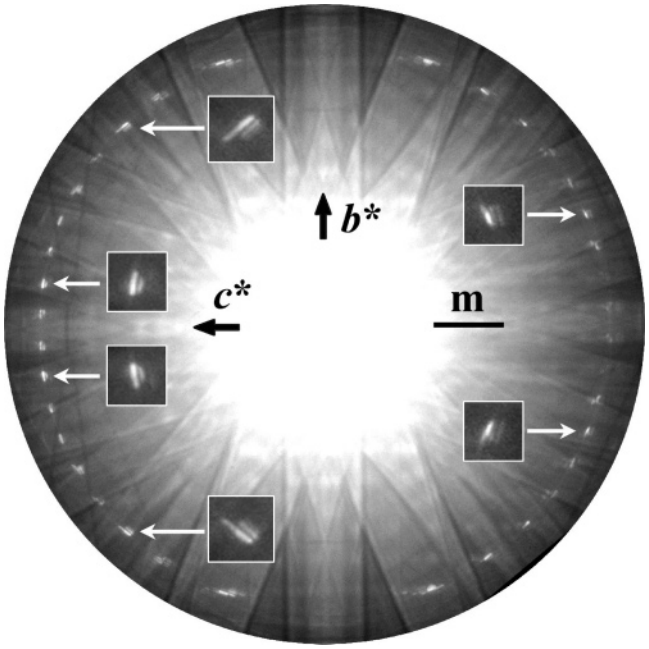

Figure 9. CBED pattern of $BiMn_{0.9}Sc_{0.1}O_3$ taken along the [100] zone axis. The HOLZ reflections (insets) clearly show the mirror-plane symmetry of this pattern perpendicular to the *b**-axis.

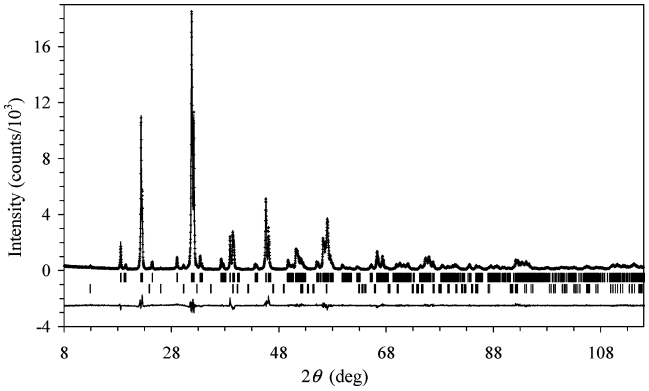

Figure 10. Observed (crosses), calculated (solid line), and difference patterns resulting from the Rietveld analysis of the laboratory X-ray powder diffraction data of $BiMn_{0.9}Sc_{0.1}O_3$ at room temperature. Bragg reflections are indicated by tick marks. The lower tick marks are given for reflections from the impurity $Bi_2O_2CO_3$ (0.8 mass %).

Table 3. Structure Parameters of $BiMn_{0.9}Sc_{0.1}O_3$ at 293 K[a]

site	Wyckoff position	*x*	*y*	*z*	*B* (Å^2)
Bi	8*f*	0.13424(10)	0.21273(13)	0.12913(14)	0.76(2)
M1[b]	4*e*	0	0.2306(7)	0.75	0.32(15)
M2[b]	4*d*	0.25	0.25	0.5	0.67(16)
O1	8*f*	0.0859(13)	0.1869(22)	0.5935(15)	1.13(18)
O2	8*f*	0.1568(15)	0.5532(23)	0.3853(18)	1.13(18)
O3	8*f*	0.3544(13)	0.5537(22)	0.1639(14)	1.13(18)

[a] Space group *C*2/*c* (No. 15); $Z = 8$; $a = 9.6029(3)$ Å, $b = 5.60988(14)$ Å, $c = 9.7690(3)$ Å, $\beta = 108.775(2)°$, and $V = 498.26(2)$ Å^3, $R_{wp} = 9.14\%$ ($S = R_{wp}/R_e = 1.81$), $R_p = 6.54\%$, $R_B = 2.70\%$, and $R_F = 1.13\%$. The occupation of all the sites is unity. [b] $g(Mn) = 0.9$ and $g(Sc) = 0.1$.

occurs below 770 K. We have found that the temperature of the magnetic phase transitions decreases and the temperature of the monoclinic-to-orthorhombic phase transition increases with increasing *x* in $BiMn_{1-x}Sc_xO_3$. The decreasing of the magnetic phase transition temperatures is in agreement with the dilution effect as observed in the $LaMn_{1-x}M_xO_3$ (M = Al, Sc, and Ga) systems.[34−36] However, it is very unlikely

Table 4. Selected Bond Lengths, *l* (Å), Angles, ϕ (deg), Bond Valence Sums (BVS), and Distortion Parameters of MnO_6 (Δ), in $BiMn_{0.9}Sc_{0.1}O_3$[a] and $BiMnO_3$[19]

		$BiMnO_3$	
	$BiMn_{0.9}Sc_{0.1}O_3$ (293 K)	300 K	550 K
Bi−O2	2.243(12)		
Bi−O1	2.293(12)		
Bi−O3	2.180(12)		
Bi−O1a	2.502(12)		
Bi−O3a	2.789(12)		
Bi−O2a	2.789(15)		
Bi−O3b	2.953(12)		
Bi−O2b	3.100(14)		
Bi−O1b	3.193(12)		
BVS(Bi)	2.90		
M1−O1 (×2)	1.972(16)	2.199(2)	2.032(3)
M1−O2 (×2)	2.051(15)	1.906(3)	2.011(4)
M1−O3 (×2)	2.109(15)	1.986(3)	2.112(4)
BVS(M1)	2.82	3.05	2.75
Δ(M1−O)	7.6×10^{-4}	37.2×10^{-4}	4.5×10^{-4}
M2−O1 (×2)	2.091(15)	1.924(2)	2.024(3)
M2−O2 (×2)	2.074(15)	2.242(2)	2.106(3)
M2−O3 (×2)	1.935(13)	1.941(2)	1.913(3)
BVS(M2)	2.92	3.05	3.09
Δ(M2−O)	11.6×10^{-4}	51.3×10^{-4}	15.4×10^{-4}
M1−O1−M2 (×2)	151.6(3)	151.4(1)	150.9(1)
M1−O2−M2 (×2)	158.9(3)	161.4(1)	158.3(1)
M1−O3−M2 (×2)	149.3(3)	149.1(1)	152.0(1)

[a] BVS = $\sum_{i=1}^{N} v_i$, $v_i = \exp[(R_0 - l_i)/B]$, *N* is the coordination number, $B = 0.37$, $R_0(Bi^{3+}) = 2.094$, and $R_0(Mn^{3+}) = 1.76$;[41] $\Delta = (1/N)\sum_{i=1}^{N} [(l_i - l_{av})/l_{av}]^2$ where $l_{av} = (1/N)\sum_{i=1}^{N} l_i$ is the average Mn−O distance.

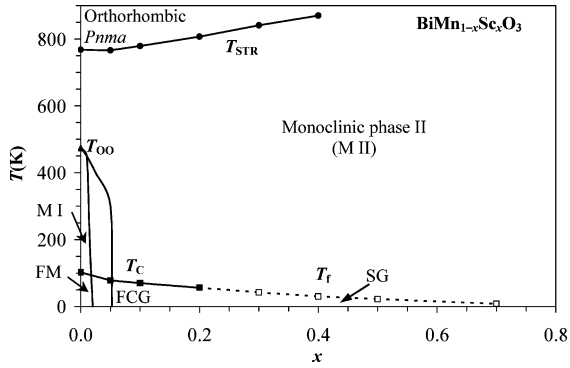

Figure 11. Phase diagram of $BiMn_{1-x}Sc_xO_3$. T_{OO} denotes the orbital ordering temperature, T_{STR} is the structural monoclinic-to-orthorhombic phase transition, T_C is the Curie temperature of ferromagnetic (FM) transition and ferromagnetic cluster-glass (FCG) transition, and T_f is the spin-glass (SG) freezing temperature.

that the orbital ordering temperature will rise with increasing content of the nonmagnetic Sc^{3+} ions in $BiMn_{1-x}Sc_xO_3$. For example, the orbital ordering temperature decreases in the $LaMn_{1-x}M_xO_3$ (M= Al, Sc, and Ga) systems with increasing *x*, and the orbital order disappears in $LaMn_{1-x}Ga_xO_3$ for $x > 0.4$.[34−36] It was shown that Sc^{3+} ions are more resistant to a cooperative static ordering of the Mn^{3+} orbitals than Ga^{3+} and Al^{3+} ions.[36] Therefore, the change in transition temperature of the monoclinic-to-orthorhombic phase transition in $BiMn_{1-x}Sc_xO_3$ with *x* gives another strong support that the orbital order in $BiMnO_3$ takes place below 474 K[19] but not below 768 K.[14]

The orbital-ordered state of $LaMnO_3$ is more stable to substitution in the Mn sublattice than that of $BiMnO_3$. This fact can be explained by the presence of magnetic frustration in $BiMnO_3$ as discussed in refs 13 and 19. The frustration also results in the much lower orbital ordering temperature

of $BiMnO_3$ ($T_{OO} = 474$ K) compared with that of $LaMnO_3$ ($T_{OO} = 750-780$ K).[34-36]

In conclusion, the effect of non-magnetic-ion substitution on the properties of $BiMnO_3$ was investigated, and the phase diagram of $BiMn_{1-x}Sc_xO_3$ was constructed (Figure 11). The orbital order in $BiMnO_3$ is destroyed by the 5% substitution of Sc for Mn. Therefore, the monoclinic-to-monoclinic phase transition is suppressed drastically by the Sc doping. The Weiss temperature is positive for all the compositions with $x < 1$, indicating that the interaction between Mn^{3+} ions is predominantly ferromagnetic. The temperature of the magnetic transitions decreases and the temperature of the structural monoclinic-to-orthorhombic phase transition increases with increasing x. The long-range magnetic order persists for $x = 0-0.2$, whereas spin-glass behavior is observed for $x > 0.3$. The crystal structure of $BiMn_{0.9}Sc_{0.1}O_3$ was investigated by the Rietveld method.

Supporting Information Available: XRD patterns of the as-prepared $BiMnO_3$ and $BiMn_{0.7}Sc_{0.3}O_3$ and after the DSC experiments up to 790 and 873 K, respectively (Figure S1), XRD patterns of $BiMn_{0.95}Sc_{0.05}O_3$ (Figure S2), the ac susceptibilities of $BiMn_{0.6}Sc_{0.4}O_3$ measured at different H_{ac} (Figure S3), the first magnetization curves in $BiMn_{1-x}Sc_xO_3$ (Figure S4), the C_p/T vs T curves of $BiMn_{0.5}Sc_{0.5}O_3$ measured at 0 and 90 kOe (Figure S5), details of the DSC curves of $BiMnO_3$ (Figure S6), and the FC $d\chi/dT$ vs T curves of $BiMn_{1-x}Sc_xO_3$ (Figure S7) (PDF). This material is available free of charge via the Internet at http://pubs.acs.org.

CM062772L